On the synergy between numerics and subgrid scale modeling in LES of stratified flows: Grid convergence of a stratocumulus-topped boundary layer

Georgios Matheou[1], Daniel Chung[2] and João Teixeira[1]

[1]Jet Propulsion Laboratory,
California Institute of Technology
georgios.matheou@jpl.nasa.gov
joao.teixeira@jpl.nasa.gov

[2]Mechanical Engineering,
University of Melbourne
daniel.chung@unimelb.edu.au

Abstract

The effectiveness of a linear upwinding scalar advection scheme to suppress numerical dispersion errors near sharp inversions in large-eddy simulations of a nocturnal stratocumulus-topped boundary layer is assessed. Linear upwinding is a trade-off between non-dissipative and non-linear positive definite advection schemes. It is shown that linear upwinding does not negatively impact the model's grid convergence properties and a sharp inversion free of numerical artifacts is maintained. Even though mean profiles and turbulence fluxes show good grid convergence characteristics the liquid water amount varies significantly with grid resolution. The entrainment rate is identical for all resolutions and independent of the liquid water amount. For the present stratocumulus case, the impact of cloud-top radiative cooling is negligible and turbulence is largely driven by convection emanating from the surface.

1 Introduction

The representation of low clouds in global circulation models is one of the largest sources of uncertainty in climate projections. The climate projection sensitivity results from the large contribution of low-cloud shortwave reflectivity in the planetary energy balance, particularly of stratocumulus (Sc) cloud decks forming over the ocean (Hartmann et al., 1992). The lack of physical understanding of the factors controlling Sc cloudiness leads to poor prediction skill. Typically, large-eddy simulations (LES) are used to gain insight into boundary layer physics and inform the development and evaluation of coarse-grained models. However, LES of Sc clouds has been challenging (e.g., Stevens et al., 2005) because: (a) the subgrid-scale modeling of stratified turbulence is inherently difficult, especially near sharp inversions, and (b) the prediction of the amount of cloud liquid requires very accurate (relative error < 0.01) prediction of specific humidity and temperature.

The present study is an extension of Matheou and Chung (2014) and aims at improving the fidelity of LES of stratified flows by considering the synergy between the numerical method and the modeling of turbulence. In Matheou and Chung (2014) the buoyancy-adjusted stretched-vortex subgrid-scale (SGS) model (Chung and Matheou, 2014) is assessed for a number of cases corresponding to diverse atmospheric boundary layer conditions. An identical model setup, including advection discretization, was used in all cases, including the Sc LES. The non-dissipative discretization in Matheou and Chung (2014) led to numerical artifacts near the Sc inversion and poor grid-convergence. Figure 1 shows the

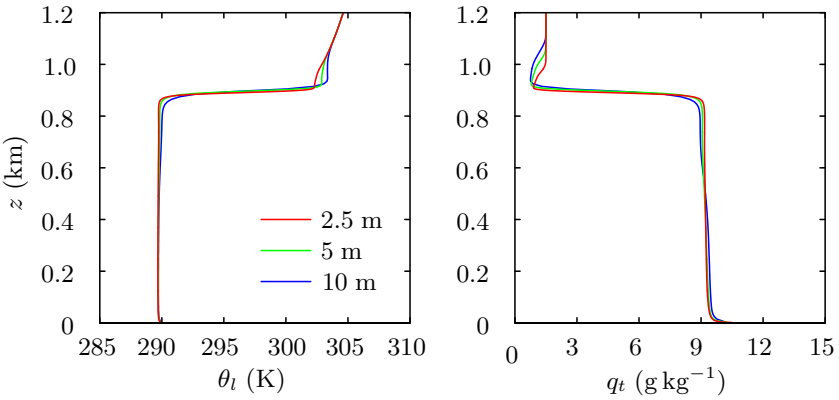

Figure 1: Vertical profiles of liquid water potential temperature, θ_l, and total water mixing ratio, q_t, of the LES of Matheou and Chung (2014) corresponding to a nocturnal stratocumulus-topped boundary layer. Profiles from three grid resolutions $\Delta x = 2.5$, 5, and 10 m are shown. The use of a non-dissipative scalar advection scheme leads to spurious under- and over-shoots near the inversion.

liquid water potential temperature and total water profiles from the LES of Matheou and Chung (2014) corresponding to the nocturnal Sc case of Stevens et al. (2005).

In very stable stratifications, there can be instances when the buoyancy affected scale L is smaller than the grid scale Δ such that the energetic motions are too small to be resolved by the grid. In an LES, this can cause the SGS model to predict nearly zero SGS fluxes. This effect is manifested as a numerical discontinuity, such as that found at a sharp inversion, and a successful LES must include considerations for both a faithful SGS model and a numerical method that handles numerical discontinuities gracefully without being overly dissipative. Figure 1 shows an instance of numerical artifacts in the form of spurious under- and over-shoots above the Sc inversion. Such violations of the local scalar boundedness are due to dispersive errors of the advection discretization and their characteristics are further discussed in Matheou and Dimotakis (2016). However, unlike the passive scalar LES runs of Matheou and Dimotakis (2016), currently, the scalar excursions affect the mean profiles and can potentially impact the global boundary layer dynamics because of the contributions of temperature and humidity to buoyancy.

To eliminate spurious scalar excursions, a common approach in simulations of geophysical flows is to use a positive definite advection scheme (e.g., Smolarkiewicz and Margolin, 1998). However, such methods can overpower and indiscriminately suppress the SGS model physics. For instance, the anisotropic character of the buoyancy-adjusted stretched-vortex model can allow horizontal mixing but suppress vertical mixing in stably stratified conditions based on the local flow dynamics. A trade-off between non-dissipative and non-linear positive definite advection is linear upwinding.

The Quadratic Upstream Interpolation for Convective Kinematics (QUICK, Leonard, 1979), a linear upwinding scheme, is presently assessed for scalar advection in LES of a Sc cloud. The case of a nocturnal Sc corresponding to the first research flight (RF01) of the second Dynamics and Chemistry of Marine Stratocumulus (DYCOMS-II) field study is simulated. To assess the performance of the model, the grid convergence properties of mean profiles, turbulence fluxes and bulk boundary layer statistics are considered for four runs with grid resolutions in 1.25–10 m. An additional run is carried out to explore the effects of cloud-top radiative cooling.

2 Large-eddy simulation model

The LES model of Matheou and Chung (2014) is used. The Favre-filtered (density-weighted) anelastic approximation of the Navier–Stokes equations (Ogura and Phillips, 1962) is numerically integrated on an f-plane ($\{\text{zonal, meridional, vertical}\} = \{x_1, x_2, x_3\} = \{x, y, z\}$). The conservation equations for mass, momentum, liquid water potential temperature, and total water, neglecting resolved-scale viscous terms, are, respectively,

$$\frac{\partial \bar{\rho}_0 \tilde{u}_i}{\partial x_i} = 0, \tag{1}$$

$$\frac{\partial \bar{\rho}_0 \tilde{u}_i}{\partial t} + \frac{\partial (\bar{\rho}_0 \tilde{u}_i \tilde{u}_j)}{\partial x_j} = -\theta_0 \bar{\rho}_0 \frac{\partial \bar{\pi}_2}{\partial x_i} + \delta_{i3} g \frac{\bar{\rho}_0 (\tilde{\theta_v} - \langle \tilde{\theta_v} \rangle_x)}{\theta_0} - \epsilon_{ijk} \bar{\rho}_0 f_j (\tilde{u}_k - u_{g,k}) - \frac{\partial \tau_{ij}}{\partial x_j}, \tag{2}$$

$$\frac{\partial \bar{\rho}_0 \tilde{\theta}_l}{\partial t} + \frac{\partial \bar{\rho}_0 \tilde{\theta}_l \tilde{u}_j}{\partial x_j} - D x_3 \frac{\partial \bar{\rho}_0 \tilde{\theta}_l}{\partial x_3} = -\frac{1}{\pi c_p} \frac{\partial F_{\text{rad}}}{\partial x_3} - \frac{\partial \sigma_{\theta,j}}{\partial x_j}, \tag{3}$$

$$\frac{\partial \bar{\rho}_0 \tilde{q}_t}{\partial t} + \frac{\partial \bar{\rho}_0 \tilde{q}_t \tilde{u}_j}{\partial x_j} - D x_3 \frac{\partial \bar{\rho}_0 \tilde{q}_t}{\partial x_3} = -\frac{\partial \sigma_{q,j}}{\partial x_j}. \tag{4}$$

The thermodynamic variables are decomposed into a constant potential temperature basic state, denoted by subscript 0, and a dynamic component. Accordingly, θ_0 is the constant basic-state potential temperature and $\rho_0(z)$ is the density. u_i and $u_{g,i}$ are the Cartesian components of the velocity vector and geostrophic wind, respectively, and $f = [0, 0, f_3]$ is the Coriolis parameter. The subgrid-scale (SGS) terms τ_{ij} and σ_j are estimated using the buoyancy adjusted stretched-vortex subgrid scale (SGS) model (Chung and Matheou, 2014). Buoyancy is proportional to deviations of virtual potential temperature from its instantaneous horizontal average, $\langle \theta_v \rangle$. π_2, the dynamic part of the Exner function,

$$\pi = \frac{\pi_0 + \pi_1 + \pi_2}{c_p} = \frac{T}{\theta} = \left(\frac{p}{p_{\text{ref}}} \right)^{\frac{R_d}{c_p}}, \tag{5}$$

enforces the anelastic constraint (1). The thermodynamic pressure, p, in each grid cell is computed from (5), the sum of the basic state Exner, $\pi_0(z)$, plus a contribution due to the deviation of the horizontal mean from the basic state, $\pi_1(t, z)$, and $\pi_2(t, x, y, z)$.

The simulation setup follows Stevens et al. (2005). The effect of the large-scale environment is included in the equations for θ_l and q_t through the subsidence terms. The large-scale horizontal divergence is currently $D = 3.75 \times 10^{-6}$ s^{-1}. The subgrid condensation scheme is "all or nothing", i.e., no partially saturated air in the grid cells. The thermodynamic state at the grid-cell center is used to classify each grid cell as saturated or not and determine the corresponding thermodynamic coefficients for all variables, including those residing at the cells vertices. All water condensate is assumed suspended (no drizzle/precipitation allowed). The net longwave radiative flux is parameterized by

$$F_{\text{rad}}(t, x, y, z) = F_0 e^{-Q(z,\infty)} + F_1 e^{-Q(0,z)} + \rho(z_i) c_p D \alpha_z [(z - z_i)^{4/3}/4 + z_i (z - z_i)^{1/3}], \tag{6}$$

where

$$Q(z_1, z_2) = \kappa \int_{z_1}^{z_2} \rho \, r_l(t, x, y, z) \, \mathrm{d}z, \tag{7}$$

r_l is the liquid water mixing ratio, and z_i the column-wise inversion height. The constant values are $F_0 = 70$ W m^{-2}, $F_1 = 22$ W m^{-2}, $\kappa = 85$ $m^2\, kg^{-1}$, and $\alpha_z = 1$ m$^{-4/3}$. The

radiation flux is calculated at each model time-step column-wise. The spatially uniform and constant in time sensible and latent heat fluxes are 15 $\mathrm{W\,m^{-2}}$ and 115 $\mathrm{W\,m^{-2}}$.

The governing equations (1–4) are discretized on an Arakawa C (staggered) grid (Harlow and Welch, 1965; Arakawa and Lamb, 1977; Matheou et al., 2011). The fully conservative four-order advection scheme of Morinishi et al. (1998) is used for momentum advection, QUICK (Leonard, 1979) is used for θ_l and q_t advection, and second-order centered differences for all derivatives associated with the SGS terms. QUICK does not enforce monotonicity of the advected scalar fields and it is less dissipative than monotone schemes (e.g., Matheou and Dimotakis, 2016). The scalar advection terms are approximated by

$$\frac{\partial u\phi}{\partial x} \approx \frac{9}{8}\frac{f_{i+1/2} - f_{i-1/2}}{\Delta x} - \frac{1}{8}\frac{g_{i+3/2} - g_{i-3/2}}{3\Delta x}, \tag{8}$$

where

$$f_{i+1/2} = u_{i+1/2}[(\phi_i + \phi_{i+1})/2 + \phi_u], \tag{9}$$

$$g_{i+1/2} = u_{i+1/2}(\phi_{i-1} + \phi_{i+2})/2. \tag{10}$$

The upwind contribution to the scalar flux is

$$\phi_u = \begin{cases} (\phi_{i-1} - 2\phi_i + \phi_{i+1})/8, & \text{if } \; u_{i+1/2} > 0 \\ (\phi_i - 2\phi_{i+1} + \phi_{i+2})/8, & \text{if } \; u_{i+1/2} < 0. \end{cases} \tag{11}$$

The computational domain is doubly periodic in the horizontal directions and all runs have a domain size of $5.12^2 \times 1.5$ km. Four runs at varying grid resolutions, $\Delta x = 1.25$, 2.5, 5 and 10 m, are used to investigate the effect of grid resolution on flow statistics. An additional run with $\Delta x = 5$ m is carried out to explore the sensitivity of convection to cloud top radiative cooling. All grids are uniform and isotropic, i.e., $\Delta x = \Delta y = \Delta z$. The highest resolution is very computationally expensive because of the fine grid (20 billion grid cells) and was only run up to $t = 2$ h. It is likely the largest LES performed to date. Table 1 summarizes the LES runs.

Table 1: Summary of LES runs. All grids are uniform and isotropic, $\Delta x = \Delta y = \Delta z$. Radiation is denoted "off" when the term in (6) is set to zero and "on" otherwise.

run	Δx (m)	**grid** ($N_x \times N_y \times N_z$)	**radiation**
A	10	$512 \times 512 \times 150$	on
B	5	$1024 \times 1024 \times 300$	on
B2	5	$1024 \times 1024 \times 300$	off
C	2.5	$2048 \times 2048 \times 600$	on
D	1.25	$4096 \times 4096 \times 1200$	on

3 Grid convergence

Figures 2 and 3 show that all flow statistics, except those associated with liquid water, exhibit good resolution independence. Mean profiles are identical for all grid resolutions. Turbulence fluxes, including turbulent kinetic energy (TKE), converge for $\Delta x < 2.5$ m. The turbulent fluxes and TKE include the SGS contribution. All flow statistics are in good agreement with the observations and are within the inter-model spread reported in

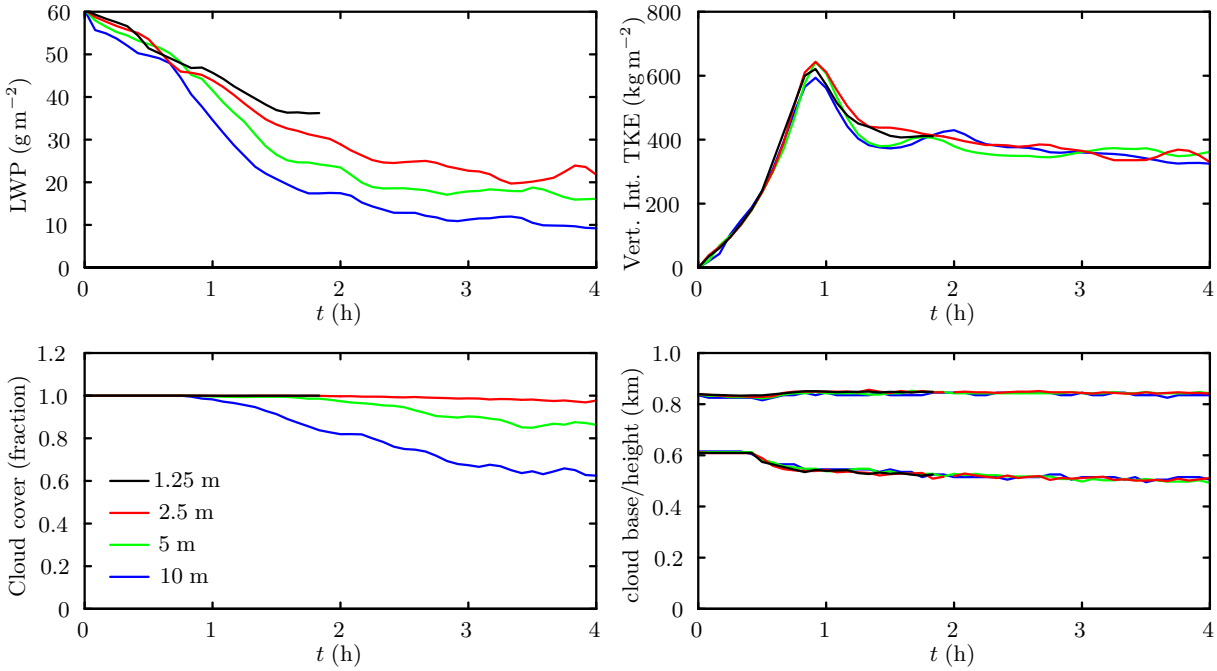

Figure 2: Grid convergence of time traces of a stratocumulus-topped boundary layer LES. The traces of liquid water path (LWP), vertically integrated turbulent kinetic energy (TKE), cloud cover, and cloud base and height are plotted for three runs with grid resolutions $\Delta x = 1.25$, 2.5, 5, and 10 m. The simulation with $\Delta x = 1.25$ was only run up to $t = 2$ h.

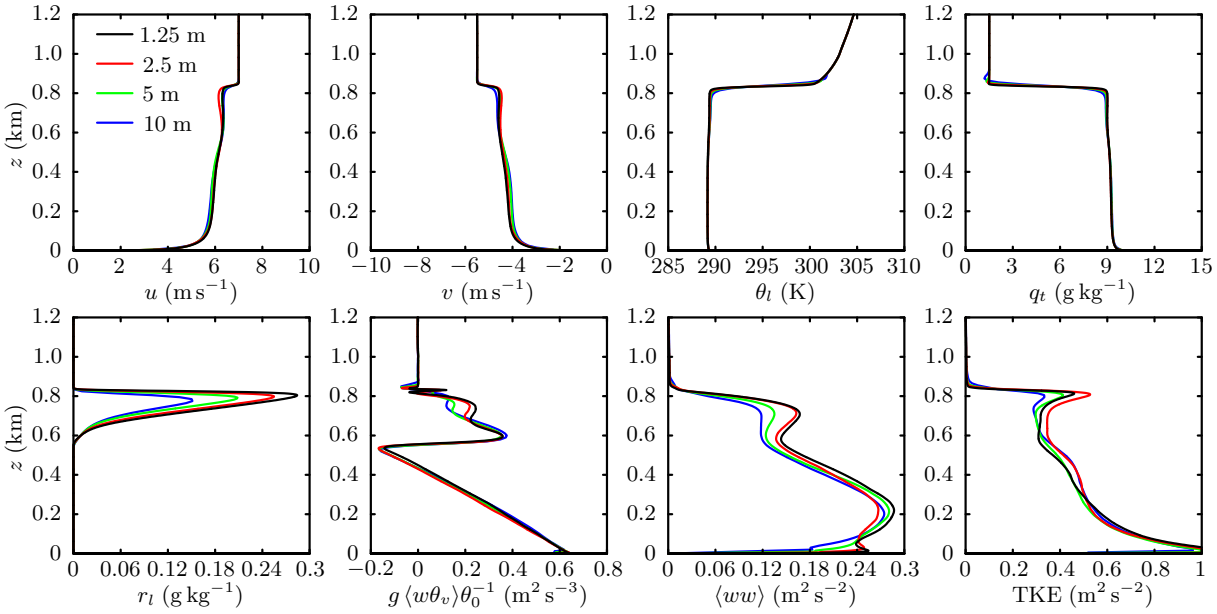

Figure 3: Grid convergence of vertical profiles of a stratocumulus-topped boundary layer LES. The profiles of zonal, u, and meridional, v, winds; liquid water potential temperature, θ_l; total water mixing ratio q_t; cloud liquid water mixing ratio r_l; buoyancy flux, $g\langle w\theta_v\rangle/\theta_0$; vertical-velocity variance, $\langle ww\rangle$; and turbulent kinetic energy are plotted for three runs with grid resolutions $\Delta x = 1.25$, 2.5, 5, and 10 m. The profiles correspond to a horizontal–time average in $t = 1.5$–2 h.

Stevens et al. (2005). Some of the numerical artifacts in the runs of Matheou and Chung (2014), reproduced here in figure 1, are significantly reduced or eliminated by the use of QUICK. In the present runs, a sharp inversion is maintained and only simulations with $\Delta x < 2.5$ m show some under- and over-shoots above the inversion.

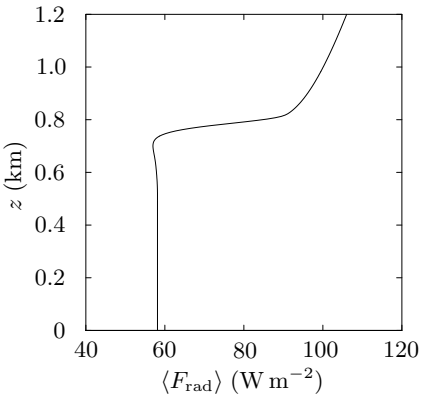

Figure 4: Horizontally averaged radiative flux, $F_{\rm rad}$, at the end of the run ($t = 4$ h) with $\Delta x = 5$ m.

The amount of liquid in each grid cell is diagnosed based on the local relative humidity, thus accurate prediction of the liquid water content requires small q_t errors ($r_l \sim 0.001 q_t$). During the first hour, a rapid reduction of liquid water path (LWP) and cloud top height is observed because the large-scale subsidence is not balanced by entrainment while turbulence is 'spinning up.' After model spin up, $t > 1$ h, entrainment and subsidence are in approximate balance resulting in a constant cloud-top height. The runs are carried out up to $t = 4$ h, but the boundary layer is not in a quasi steady state (e.g., Chung et al., 2012), which can affect the relative contributions of the various driving mechanisms.

4 Entrainment, liquid water path, and cloud-top radiative cooling

Even though the prediction of the amount of cloud liquid requires very fine resolutions, the entrainment rate and cloud layer thickness are identical in all runs (do not depend on LWP). This suggests that the role of cloud-top radiative cooling is not significant in driving the boundary layer turbulence. Accordingly, a pair of simulations with and without radiation parameterization are carried out to test this inference. Figure 4 shows the horizontal mean of $F_{\rm rad}$ at $t = 4$ h for the $\Delta x = 5$ m run and figure 5 compares the traces of a pair of $\Delta x = 5$ m runs with and without radiation fluxes. The differences between the two runs is negligible. The vertical profiles (not shown) are also very similar.

Moreover, the buoyancy flux profile in figure 3 and flow visualizations, such as the q_t contours shown in figure 6, suggest that the boundary layer is driven by convection emanating from the surface, rather than radiative cooling at the cloud top. Cloud top radiative cooling is expected to have a significant impact on the Sc turbulence dynamics. For instance: "stratocumulus is usefully defined as a low-level cloud system whose dynamics are primarily driven by convective instability caused by cloud-top radiative cooling" (Wood, 2012). The linearly decreasing with respect to height buoyancy flux with significant negative values implies a decoupled boundary layer structure (Bretherton, 1997). This appears to contradict the well-mixed structure of temperature and humidity and is perhaps unexpected in a shallow boundary layer (presently $z_i \approx 800$ m).

5 Conclusion

Modern LES models can accurately capture multi-physics stratified flows with sharp stable interfaces and achieve grid convergence. In spite of the good model performance, many

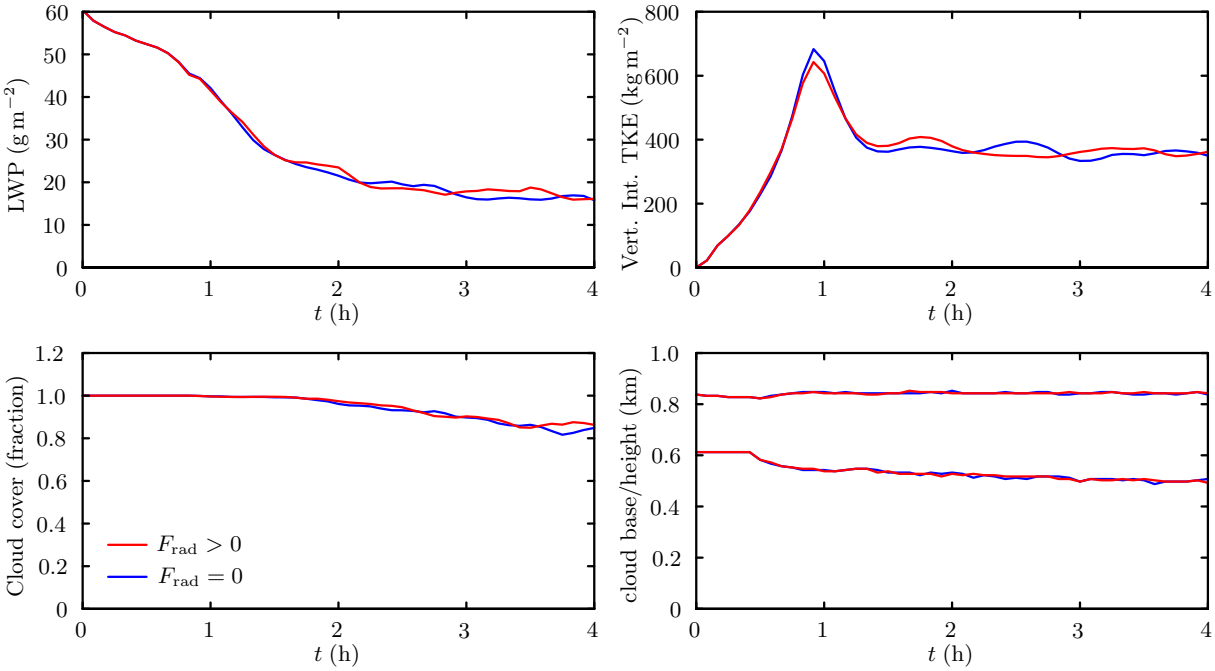

Figure 5: Time traces of a pair of $\Delta x = 5$ m-runs with and without radiation.

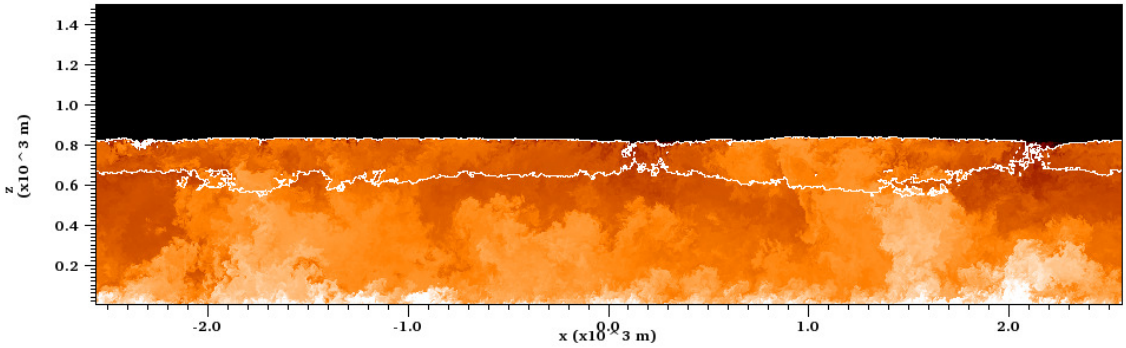

Figure 6: Total water mixing ratio contours (color) on a vertical cross-section at $t = 2$ h from the high resolution run $\Delta x = 1.25$ m. The white contour corresponds to the cloud boundary.

questions remain regarding the dynamics of stratocumulus-topped atmospheric boundary layers. It is envisioned that the present advances in model performance in combination with observations will further elucidate more aspects of this important flow.

Acknowledgements

We acknowledge the support provided by the Office of Naval Research, Marine Meteorology Program, the NASA MAP Program and the NOAA/CPO MAPP Program. Part of this research was supported by U.S. Department of Energy, Office of Biological and Environmental Research, Earth System Modeling and DOE Grant DE-NA0002382. Computational resources supporting this work were provided by the JPL Office of the Chief Information Officer and the NASA High-End Computing (HEC) Program through the NASA Advanced Supercomputing (NAS) Division at Ames Research Center. Part of this research was carried out at the Jet Propulsion Laboratory, California Institute of Technology, under a contract with the National Aeronautics and Space Administration.

References

Arakawa, A. and Lamb, V. R. (1977). Computational design of the basic dynamical processes of the UCLA general circulation model. In *Methods of Computational Physics*, volume 17, pages 173–265. Academic Press.

Bretherton, C. S. (1997). Convection in stratocumulus-topped atmospheric boundary layers. In *The Physics and Parameterization of Moist Atmospheric Convection*, pages 127–142. Springer.

Chung, D. and Matheou, G. (2014). Large-eddy simulation of stratified turbulence. Part I: A vortex-based subgrid-scale model. *J. Atmos. Sci.*, 71:1863–1879.

Chung, D., Matheou, G., and Teixeira, J. (2012). Steady-state large-eddy simulations to study the stratocumulus to shallow-cumulus cloud transition. *J. Atmos. Sci.*, 69:3264–3276.

Harlow, F. H. and Welch, J. E. (1965). Numerical calculation of time-dependent viscous incompressible flow of fluid with free surface. *Phys. Fluids*, 8(12):2182–2189.

Hartmann, D. L., Ockert-Bell, M. E., and Michelsen, M. L. (1992). The effect of cloud type on Earth's energy balance: Global analysis. *J. Climate*, 5(11):1281–1304.

Leonard, B. P. (1979). A stable and accurate convective modelling procedure based on quadratic upstream interpolation. *Comput. Methods in Appl. Mech. Eng.*, 19(1):59–98.

Matheou, G. and Chung, D. (2014). Large-eddy simulation of stratified turbulence. Part II: Application of the stretched-vortex model to the atmospheric boundary layer. *J. Atmos. Sci.*, 71(12):4439–4460.

Matheou, G., Chung, D., Nuijens, L., Stevens, B., and Teixeira, J. (2011). On the fidelity of large-eddy simulation of shallow precipitating cumulus convection. *Mon. Weather Rev.*, 139:2918–2939.

Matheou, G. and Dimotakis, P. E. (2016). Scalar excursions in large-eddy simulations. *J. Comput. Phys.* submitted.

Morinishi, Y., Lund, T. S., Vasilyev, O. V., and Moin, P. (1998). Fully conservative higher order finite difference schemes for incompressible flow. *J. Comput. Phys.*, 143(1):90–124.

Ogura, Y. and Phillips, N. A. (1962). Scale analysis of deep and shallow convection in the atmosphere. *J. Atmos. Sci.*, 19:173–179.

Smolarkiewicz, P. K. and Margolin, L. G. (1998). MPDATA: A finite-difference solver for geophysical flows. *J. Comput. Phys.*, 140(2):459–480.

Stevens, B., Moeng, C.-H., Ackerman, A. S., Bretherton, C. S., Chlond, A., De Roode, S., Edwards, J., Golaz, J.-C., Jiang, H. L., Khairoutdinov, M., Kirkpatrick, M. P., Lewellen, D. C., Lock, A., Muller, F., Stevens, D. E., Whelan, E., and Zhu, P. (2005). Evaluation of large-eddy simulations via observations of nocturnal marine stratocumulus. *Mon. Weather Rev.*, 133:1443–1462.

Wood, R. (2012). Stratocumulus clouds. *Mon. Weather Rev.*, 140:2373–2423.